Received: 15 May 2020 | Accepted: 30 August 2020

DOI: 10.1002/vzj2.20069

Vadose Zone Journal

ORIGINAL RESEARCH ARTICLE

Volume-related quantification of organic carbon content and cation exchange capacity of macropore surfaces in Bt horizons

Martin Leue[1] | **Daniel Uteau**[2] | **Stephan Peth**[2] | **Steffen Beck-Broichsitter**[1] | **Horst H. Gerke**[1]

[1] Leibniz-Centre for Agricultural Landscape Research (ZALF), Research Area 1 Landscape Functioning, Eberswalder Str. 84, Müncheberg D-15374, Germany

[2] Faculty of Ecological Agriculture, Dep. of Soil Science, Univ. Kassel, Nordbahnhofstr. 1a, Witzenhausen D-37213, Germany

Correspondence
Martin Leue, Leibniz-Centre for Agricultural Landscape Research (ZALF), Research Area 1 Landscape Functioning, Eberswalder Str. 84, D-15374 Müncheberg, Germany.
Email: Martin.Leue@zalf.de

Funding information
Deutsche Forschungsgemeinschaft, Grant/Award Numbers: GE 990/14, LE 3177/1-2

Abstract

In structured soils, earthworm burrows, root channels, shrinkage cracks, and interaggregate spaces form complex macropore networks relevant for preferential transport, turnover processes, and root growth. Macropore walls are often coated with organomineral material, which determine physicochemical properties such as wettability, sorption, and the cation exchange capacity (CEC). The objective here was to identify volume-averaged mean macropore coating properties of larger intact soil cores (~7,500 cm^3) from Bt horizons of Luvisols developed from loess and glacial till. The quantification of organic C (OC) content and CEC of macropore surfaces was based on three-dimensional images of X-ray computed tomography (XRCT) of 231-μm voxel resolution and a vesselness procedure to distinguish between biopores and cracks. Macropore surface areas were combined with millimeter-scaled data of OC contents and CEC of macropore coating material. The surface of macropores that accounted for 5.6 % (loess-Bt) and 4.6 % (till-Bt) of the samples' volumes represented approximately one-third of the OC content and CEC of the bulk soil. Among the macropores, surfaces of larger biopores contributed most to OC content of the soil cores. The contribution of coated cracks and pinhole fillings to OC content was larger for the till-Bt than for the loess-Bt. Locally higher OC contents and CEC values emphasize the role of macropore surfaces in Bt horizons of Luvisols as geochemical hotspots and for mass exchange, especially during preferential flow and transport. Volume-based coating properties may help improving macroscopic-scale two-domain flow and transport models.

1 | INTRODUCTION

In structured soils, earthworm burrows, root channels, shrinkage cracks, and interaggregate pore spaces form

Abbreviations: 3D, three-dimensional; CEC, cation exchange capacity (effective); CLSM, confocal laser scanning microscope; OC, organic carbon; OM, organic matter; 2D, two-dimensional; vx, voxel; XRCT, X-ray computed tomography.

complex macropore networks. These pore networks are relatively persistent, particularly in the subsoil (Pagenkemper, Peth, Uteau-Puschmann, & Horn, 2013; Zhang et al., 2018), where they represent biogeochemical hotspots (Bundt, Widmer, Pesaro, Zeyer, & Blaser, 2001; Kuzyakov & Blagodatskaya, 2015) and serve as preferential pathways for water movement (Jarvis, 2007) and plant roots (Kautz, 2015; Ruiz, Or, & Schymanski, 2015). Macropore surfaces provide an effective interface area (Gerke, 2012) for sorption and exchange processes of preferentially transported chemicals (Fér et al., 2018; Lin, 2010). The macropore–matrix mass exchange across these interfaces depends on morphological characteristics (i.e., pore geometries) and physicochemical properties such as the clay content and mineralogy (Beck-Broichsitter, Gerriets, Gerke, et al., 2020) of the macropore surfaces.

In particular, the clay-illuvial horizons of Luvisols (Bt horizons) feature characteristic clay-organic coatings along the surfaces of aggregates, biopores, and cracks. It is proven for the surfaces of earthworm burrows (Don et al., 2008; Pagenkemper et al., 2015), as well as for cracks (Leue, Wohld, & Gerke, 2018), that these coatings contain increased organic C (OC) contents. However, differences in the organic matter (OM) composition (e.g., aliphatic and heterocyclic compounds) were found between biopore coatings and clay-organic crack coatings, as well as pore fillings ("pinholes") (Leue, Eckhardt, Ellerbrock, Gerke, & Leinweber, 2016; Leue, Eckhardt, Gerke, Ellerbrock, & Leinweber, 2017). Macropore type-specific differences were also proven for the effective cation exchange capacity (CEC) of intact macropore surfaces (Leue, Beck-Broichsitter, Felde, & Gerke, 2019). This indicates differences between biopores and cracks (including fissures, small disconnected pores, and interaggregate spaces) with respect to matter transport and turnover. Thus, a separate consideration of the two main macropore types (i.e., biopores and cracks) is required for an improved quantification of macropore effects on (preferential) transport and turnover processes. Leue et al. (2018) and Leue, Beckbroichsitter, et al. (2019) manually separated the outermost layer of intact macropore surfaces from Bt horizons. The OC content and CEC values were determined in the separated material, and their two-dimensional (2D) spatial distribution along intact macropore surfaces was determined using diffusive infrared spectroscopy ("DRIFT mapping"). For these samples of 6- to 12-cm edge length, the millimeter-scale OC contents varied locally between 0.2 and 2.7 % (loess-Bt) and between 0.15 and 1.4 % (till-Bt). Levels of OC contents (and similarly also for the CEC) increased in the order of coated cracks, pinhole fillings, and biopore walls as compared with the soil matrix. Although X-ray computed tomography (XRCT) data could be used for a core-scale separation of two major macropore surface types (Leue, Beck-Broichsitter, et al., 2019), the determination of macropore surface properties in intact cores of larger volumes remained an open question.

Core Ideas

- Macropores are hotspots for biogeochemical and exchange processes in soils.
- Quantification of OC content and CEC along macropore surfaces in soil cores.
- Combination of XRCT-based macropore surfaces morphologies with OC and CEC data.
- Macropore surface volumes (4–6 %) account for one-third of the OC content and CEC.
- Macropore–matrix properties are crucial for modeling preferential transport.

For describing preferential flow and transport processes with continuum approaches in macroporous soils, macroscopic scale (i.e., volume-averaged) parameters (Gerke, 2012) that represent effective properties of macropore surfaces such as clay and OC within a defined soil volume of interest (e.g., soil horizon) are required. For the exchange terms in two-domain models (Gerke, 2006; Gerke & van Genuchten, 1993), such volume-related effective parameters are highly useful. They characterize all physical and chemical properties of the macropore–matrix interface relevant for mass exchange of nonsorbing and sorbing chemicals (Haas, Horn, Ellerbrock, & Gerke, 2020) that is depending on the properties, surface area, and geometry of macropores that actively participate in the transport of solutes during preferential flow events (Gerke, Dusek, & Vogel, 2013).

The XRCT in combination with quantitative three-dimensional (3D) image analysis has frequently been used to investigate intact soil structures and macropore networks noninvasively (Pagenkemper et al., 2015; Sammartino et al., 2015; Perret, Prasher, Kantzas, & Langford, 1999; Pierret, Capowiez, Belzunces, & Moran, 2002). In binary 3D image datasets, a separation between macropore types can be achieved (e.g., by volume thresholding; Capowiez, Sammartino, & Michel, 2011; Pagenkemper et al., 2013, 2015) and shape parameters (Leue, Ulteau-Puschmann, et al., 2019; Zhang, Peng, Zhou, Lin, & Sun, 2015, 2018). Leue, Ulteau-Puschmann, et al. (2019) developed an image processing workflow to separate biopores from shrinkage cracks and interaggregate spaces. This workflow can be applied to XRCT data obtained from large soil cores (25-cm height, 20 cm in diam.) which provide relatively representative information on soil structure. In particular, the calculated surface area could be used to

quantify OC and CEC data obtained from earlier 2D measurements at macropore surfaces (Leue et al., 2018; Leue, Beck-Broichsitter, et al., 2019) for soil volumes of core samples or soil horizons.

Keck, Strobel, Gustafsson, and Koestel (2017) determined the CEC of small soil cores by localizing and quantifying the spatial distribution of adsorbed cations in XRCT data using Ba^{2+} as a contrast agent and compared these CEC values with those determined by standard batch analysis. Although they did not obtain a 1:1 relationship and noted under- and overestimations in specific cases, Keck et al. (2017) found a significant correlation between CEC values obtain by XRCT and conventional laboratory data (batch experiments). This suggests a potential of the method to extrapolate conventionally measured CEC values into 3D pore spaces, which is expected to result in more realistic soil system models. The soil core size of 22 mm in diameter used by Keck et al. (2017) enabled a relatively high XRCT spatial resolution (voxel edge length of 20 μm), which was sufficient to quantify the cation adsorption sites via gray value thresholding. Regarding soil structural pores such as biopores and cracks, a core size of 22 mm is not sufficiently representative for the pore network within soil horizons. The soil core size should therefore cover larger soil volumes. However, XRCT measurements of larger soil cores result in much coarser spatial resolutions in the order of >200 μm (Leue, Ulteau-Puschmann, et al., 2019; Pagenkemper et al., 2015). In this case, the approach of Keck et al. (2017) would not be applicable since submillimeter-scaled locations of cation absorption sites, as well as of OC enrichments in clay-organic coatings, cannot be spatially resolved. Nevertheless, the extrapolation of OC and CEC data via the summed surface area of the identified macropores may be validated by comparing OC and CEC values of the soil matrix (excluding the macropore surfaces) with those of the bulk soil. On the basis of the cited literature and our own previously published studies on OC and CEC distribution along macropore walls (Leue et al., 2018, Leue, Beck-Broichsitter, et al., 2019), we assume a disproportionally high quantitative relevance of macropore surfaces vs. bulk soil for OC and CEC in structured soils. We further assume that the quantities of both parameters can be calculated for soil volumes (i.e., three-dimensionally extrapolated) when combined with morphological data on the macropore surfaces.

The objective of this work was to quantify the OC content and CEC of macropores surfaces in soil cores of 25-cm height and 20 cm in diameter, obtained from Bt horizons of two Luvisols developed on loess and glacial till as parent material. We improved the macropore type separation algorithm (Leue, Ulteau-Puschmann, et al., 2019) and combined 3D images from XRCT measurements with earlier published data of OC (Leue et al., 2018) and CEC (Leue, Beck-Broichsitter, et al., 2019) of separated and intact macropore material from the same sites. The OC and CEC quantities of macropore surfaces were compared with data obtained for the pure soil matrix and bulk soil samples in order to check the consistency of the approach and to prospectively enable the consideration of macropore type-specific surface properties in transport and turnover models.

2 | MATERIAL AND METHODS

2.1 | Concept

With respect to the outlined differences in OC and CEC of soil matrix (Mx), biopores (Biop), cracks (Cr), and pinhole (PIN) fillings, each of these pore types and soil components (Figure 1) was considered separately.

In the conceptual workflow (Figure 2), the macropore surface area was calculated separately for biopores and cracks from intact soil cores from Bt horizons (details in Section 2.2) using 3D images from XRCT (details in Sections 2.3 and 2.4). The previously determined, macropore-type specific OC contents (Leue et al., 2018) and CEC data (Leue, Beck-Broichsitter, et al., 2019; see Section 2.5) were quantified according to mean macropore wall thickness data (details in Section 2.6). Finally, the total amount of OC and CEC for all macropore surfaces of the soil cores was calculated macropore type-specific (details in Section 2.7) using the macropore surface area, the surface layer thickness, the OC and CEC values, and the bulk density.

We considered the material manually separated from macropores as a first approximation of the outermost macropore layer with visually present organic and clay-organic coatings. A different sampling strategy was necessary for "pinholes," defined as individual disconnected or tapped blind holes (Leue et al., 2016). Their surface area could not be calculated from 3D images due to their often small sizes in relation to the relatively coarse XRCT scanning resolution and their similarity in bulk density as compared with the soil matrix. Thus, pinholes were treated separately (details in Section 2.7).

2.2 | Soil properties and sample preparation

Soil samples were collected from Bt horizons of two Haplic Luvisols (IUSS Working Group WRB, 2006) under arable land use. The Luvisol developed from loess was located in northern Bohemia (Hnevceves, near Hradec Kralove, Czech Republic; 50°18′47″ N, 15°43′03″ E; mean annual precipitation = 618 mm; mean annual temperature

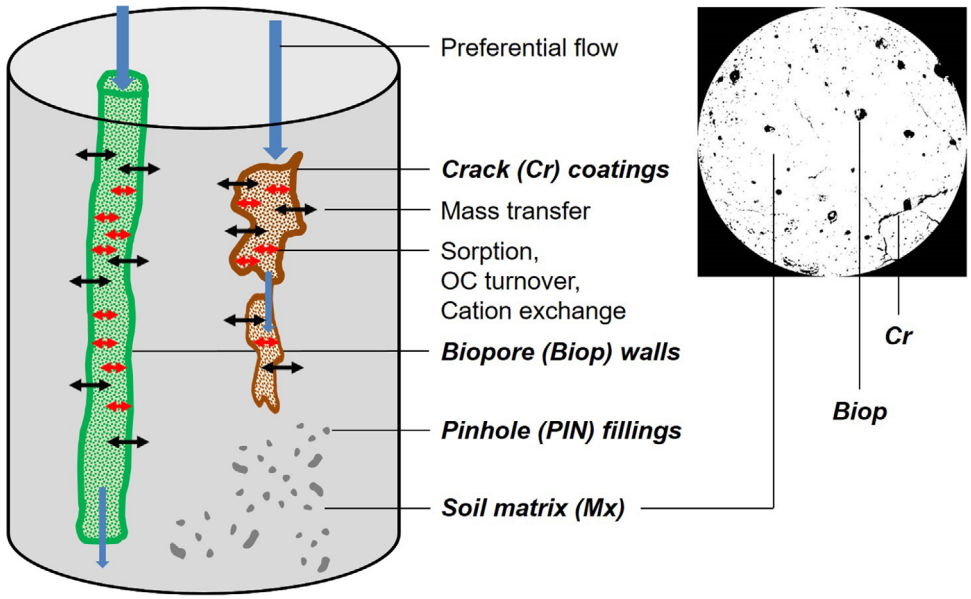

FIGURE 1 Left side: concept of macropore types in Bt horizons of Luvisols with biopores (green), coated cracks (brown), and pinhole fillings (dark gray). Right upper corner: slice of a three-dimensional image obtained from a glacial till-derived Bt horizon sample (diameter = 182 mm) after segmentation including cracks and biopores (blacks) and the porous soil matrix (white). Pinhole fillings not segmented from X-ray computed tomography (XRCT) scans (for details, see text). OC, organic C

TABLE 1 Soil physical and chemical properties of the Haplic Luvisols developed on loess (Hnevceves) and glacial till (Holzendorf). Mean values of three replicates

Horizon	Depth	Clay]	Silt	Sand	SOC
	cm	mass %			
Loess					
Ap1(L)	0–25	18.2	66.5	15.2	1.05
Ap2(L)	25–34	21.5	39.6	38.9	0.66
Bt1(L)	34–57	29.4	61.4	9.2	0.48
Bt2(L)	57–85	27.0	69.2	3.8	0.28
Bt-Cv(L)	85–96	25.6	70.0	4.4	n.d.
Cv(L)	>96	22.5	72.4	5.1	0.20
Glacial till					
Ap1(T)	0–25	9.6	29.4	60.9	0.82
Ap2(T)	25–38	12.4	25.7	61.9	0.64
Bt(T)	38–60	20.5	24.9	54.6	0.34
Cv(T)	>68	13.9	26.3	59.8	0.15

Note. SOC, soil organic C; n.d., not determined; (L), loess; (T), glacial till. For details, see Leue et al. (2018) and Leue, Beck-Broichsitter, et al. (2019).

= 8.5° C; Table 1). The Luvisol developed from glacial till was located in northeastern Germany (Holzendorf, near Prenzlau, Uckermark region; 53°22′45″ N, 13°47′11″ E; mean annual precipitation = 501 mm; mean annual temperature = 8.7 ° C; Table 1).

At the sampling sites, the top soil (Ap horizon) was removed. A parallel soil pit was excavated to facilitate the sampling and to identify the soil horizons. An acrylic glass cylinder of 25-cm height and 20-cm i.d., complemented by a steel cutting rim at the bottom, was set at the plane upper border of the Bt horizon (Loess-Luvisol: Bt1 horizon). Below the intended place, a soil monolith with slightly larger dimensions than the cylinder was excavated manually by carefully digging and scraping off surrounding soil material (Rogasik, Weinkauf, & Seyfarth, 1997). A three-legged steel frame with a holding fixture for the acrylic glass cylinder was installed around the excavated soil monolith in an exactly perpendicular position. The

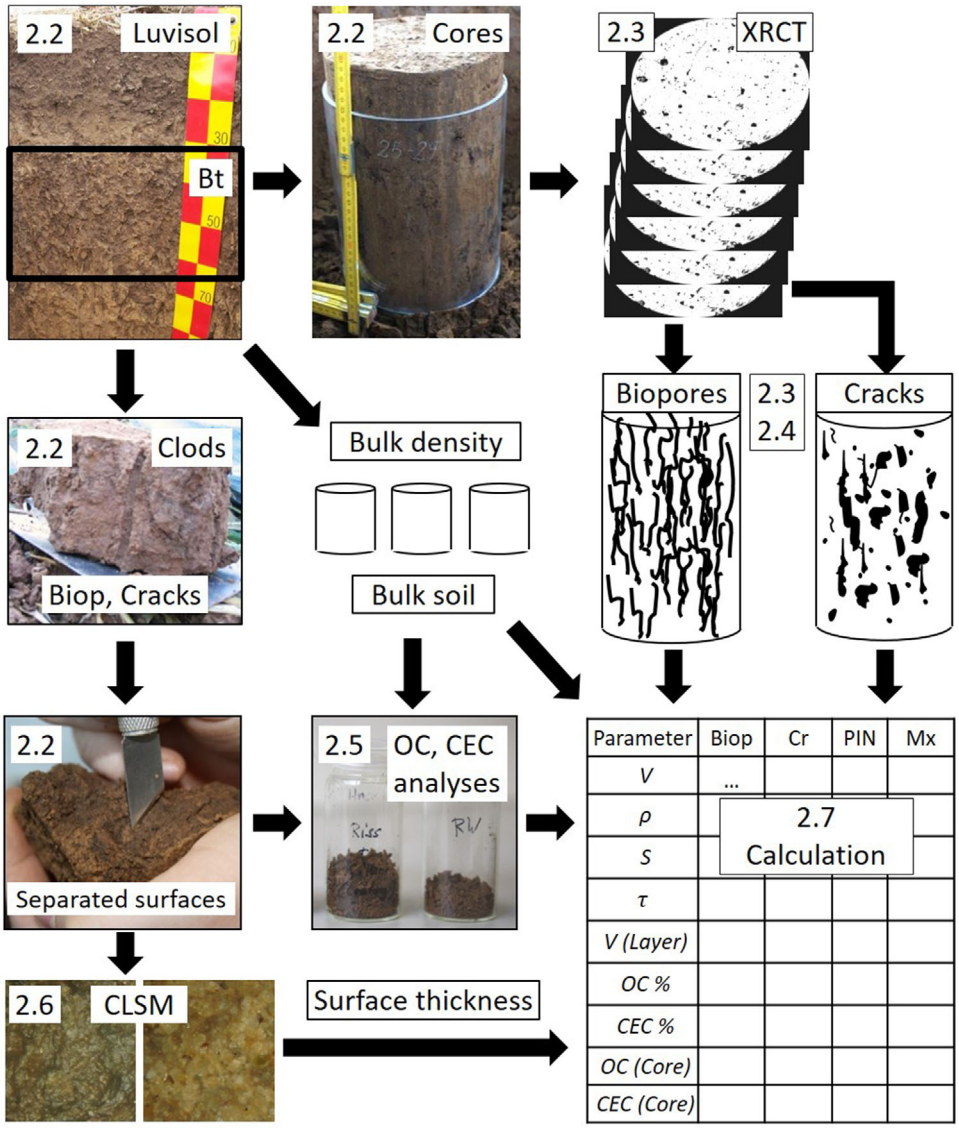

FIGURE 2 Scheme of the quantification workflow. Soil cores (top), soil clods with intact macropores (left), and small cylinders for bulk density determination (center) were sampled from the same site. Three-dimensional images obtained by X-ray computed tomography (XRCT) of the soil cores yielded macropore type-specific physical parameters (volume, surface area); numbers are equal to methods chapters. Biop, biopores; CLSM, confocal laser scanning microscopy; Cr, cracks; PIN, pinhole fillings; Mx, (soil) matrix; OC, organic C; CEC, cation exchange capacity; *V*, volume; ρ, bulk density; *S*, surface area; τ, tortuosity

steel frame allowed to press the cylinder straight downwards into the soil. During this procedure, carried out manually in one step by the help of two persons, the cutting rim removed the overhanging material. The quality of the procedure could be easily assessed due to the transparency of the cylinder wall. After the removal of the cutting rim, supernatant soil material was cut off from the lower cylinder rim. The top and bottom of the cylinders were covered by plastic caps and adhesive tape in order to fix the soil material and to prevent from desiccation. The soil cores were stored at 4 °C in the dark. Additionally, five soil cores of 100-cm^3 volume were taken per Bt horizon next to the sampling area in order to determine the soil bulk density.

2.3 | XRCT measurements and image analyses

The XRCT scanning procedure was the same as described in Leue, Ulteau-Puschmann, et al. (2019). Briefly, the field-moist soil cores were scanned with an industrial microfocus X-ray micro-tomograph (v|tome|x L 240 μCT scanner, GE-Sensing Technologies) at the Institut für Forschung und Transfer (RIF). The X-ray photon energy was set to 160 keV with a current of 1,000 μA. A number of 1,200 cone-beam projections was collected at a full rotation. A 1-mm Cu pre-filter was used to minimize beam hardening. Each soil core was scanned in two height steps resulting in

two overlapping 3D image datasets that were subsequently reconstructed to obtain a single 3D core volume. For reconstruction, the software datos|x, version 1.5.0.15 (GE Sensing Technologies) was used, which is based on a modified Feldkamp algorithm (Feldkamp, Davis, & Kress, 1984). A spatial resolution in terms of an isotropic voxel (vx) edge length of 231 μm was achieved for all samples.

All image pre- and post-processing was done with the software MAVI (Modular Algorithms for Volume Images) implemented in ToolIP (Tool for Image Processing; Fraunhofer ITWM, 2012). About 9 mm of the outermost layer of the soil cores were masked out to remove the cylinder wall, as well as possibly disturbed soil pore space close to the wall (Leue, Ulteau-Puschmann, et al., 2019). Cone artifacts due to beam hardening were corrected by applying a mean correction filter in radial direction. The correction was carried out slice by slice to compensate for the radial gradient in mean gray values.

The image analysis procedure used in Leue, Ulteau-Puschmann, et al. (2019) was improved by applying a multiscale vessel enhancement filtering to the filtered grayscale images, according to an algorithm developed by Frangi, Niessen, Vincken, and Viergever (1998) based on previous work by Sato et al. (1998). Briefly, the Hessian matrix (i.e., the second order local structure) of the image was examined to segment objects according to its vesselness. The latter is defined by Frangi et al. (1998) on the basis of the eigenvalues of the Hessian matrix. The algorithm evaluates two ratios (R_B and R_A) to define whether the object is blob-like, plate-like, or line-like. This is done recursively across different scales to take differently sized objects into account. The result is a grayscale probability map of the vesselness of dark (or bright) objects. For this study, we considered that all objects with a probability >99% are considered line-like and thus associated to the biopore dataset of each soil core. Note that the dataset of biopores includes earthworm burrows as well as root channels. For binarization of the gray value images, a global threshold was calculated for each slice, using Otsu's method (Otsu, 1979). The datasets consisted of 997–1,063 slices per soil core (i.e., core heights ranged between 230 and 245 mm).

For each of the labeled biopore and crack objects, the volume (V) and surface area (S), the size in terms of the elongation (x, y, and z dimension), the diameter (mean and SD), and the integral of mean curvature (IMC) were calculated as object features using the MAVI software. The surface-to-volume ratio (S/V) was calculated for each macropore object; the tortuosity (τ) was calculated as dimensionless parameter for each of the i numbers of N identified pore objects (PO), as the ratio between actual macropore length (vx edge length), represented by IMC, to the total length, represented by the maximum elongation

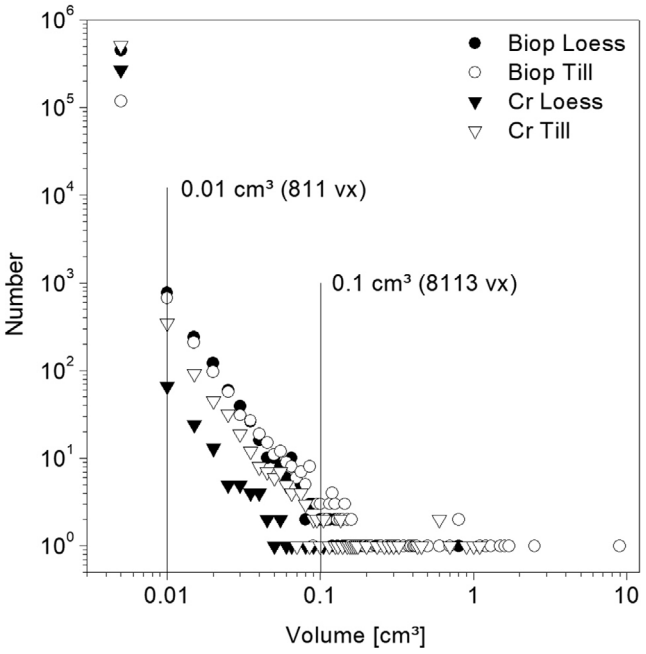

FIGURE 3 Number of identified objects vs. object volume for biopores (Biop) and cracks or interaggregate pores (Cr); mean values of counts for each of the three core samples from Bt horizons of loess- and till-derived Luvisols. The vertical lines denote the threshold values at volume (V) = 0.01 cm^3 (V = 811 voxels [vx]) and V = 0.1 cm^3 (V = 8,113 vx) for defining the macropore size classes "medium" and "large"

of an object (vx edge length) in either the x, y, or z dimension (Luo, Lin, & Li, 2010) as

$$\tau_i = \frac{\mathrm{IMC}_i}{\max\limits_{1\le i\le N} \mathrm{PO}_i(x,\ y,\ z)} \tag{1}$$

The equivalent hydraulic radius (EHR) of an identified pore object, PO_i, was similarly calculated (Luo et al., 2010) as

$$\mathrm{EHR}_i = V_i \Big/ \max_{1\le i\le N} \mathrm{PO}_i(x,y,z) \tag{2}$$

where V is the volume (in vx) and the maximum elongation of a pore object (max PO_i in vx) is in either x, y, or z dimension.

2.4 | Object size classes

Histograms of object (i.e., pore) volumes (Pagenkemper et al., 2013) were used to determine thresholds between pore volume classes (Figure 3). The idea was to quantify the significance of large pores, in which preferential flow will take place predominantly, for OC content and CEC of

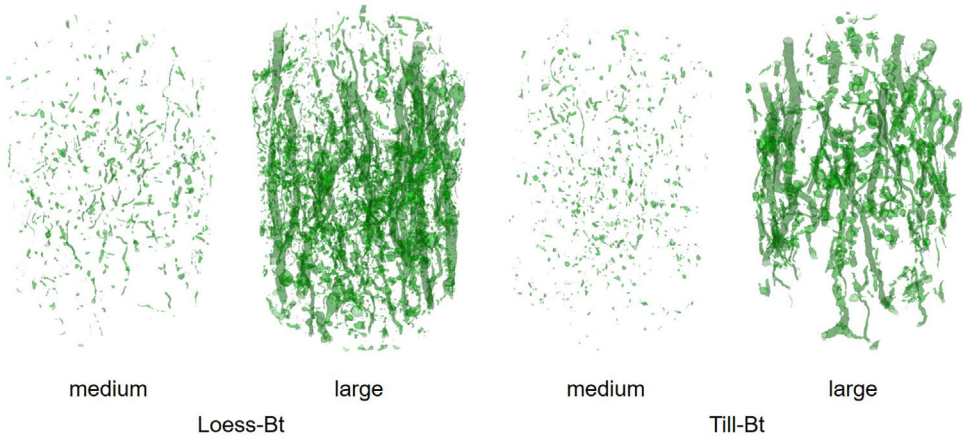

FIGURE 4 Visualization of separated macropore volume size classes for medium (>0.01 to ≤0.1 cm^3) and large (>0.1 cm^3); biopores for soil cores of 25-cm height and 20 cm in diameter (18.2 cm after image processing) from the loess-Bt (left) and the till-Bt (right)

the soils. Objects with V of >0.01 to ≤0.1 cm^3 (811–8,113 vx) were denoted as medium and pores, with $V > 0.1$ cm^3 as large. The threshold of $V = 0.01$ cm^3 ($V = 811$ vx) excluded very small objects, which often consist of voxels not exactly segmented as pores or solid matrix ("noise"). The threshold of $V = 0.1$ cm^3 ($V = 8{,}113$ vx) was determined at a region were the slope of the counts decreased strongly (Figure 3). The visual inspection of the 3D images confirmed that this threshold denoted a relatively small number of larger objects including earthworm burrows (Figure 4).

2.5 | Soil organic carbon and cation exchange capacity

Briefly, the previously published analyses of soil OC (Leue et al., 2018) and CEC at intact macropore surfaces (Leue, Beck-Broichsitter, et al., 2019) were carried out with soil clod samples from the Bt horizons collected close to the intact core sampling positions (Figure 2). The outermost surfaces of macropores, categorized into earthworm burrows, cracks with and without clay-organic coatings, "pinholes" (i.e., the black filling material of disconnected pores), and earthworm casts were manually separated from the bulk soil matrix using a scalpel (for more details on the method, see Section 4). The OC content of the samples with masses between 1.5 and 4.0 mg (obtained from surface areas of each 6.4 × 6.4 mm) was determined by elemental isotope ratio mass spectrometry (EA-IRMS, EA: Flash EA 1112, MS: Delta V Advantage, Thermo Fisher Scientific) (Leue et al., 2018). The CEC values were determined by the barium chloride batch method (Barton & Karathanasis, 1997; Blakemore, Searle, & Daly, 1987) that has been adapted to small sample masses of ~0.5 g obtained from the macropore surfaces (Leue, Beck-Broichsitter, et al., 2019).

2.6 | Microscopic analysis of macropore surfaces

A confocal laser scanning microscope (CLSM, Keyence VK-X100K, Keyence Company) was used to determine the mean layer thickness that was removed when manually separating the macropore surfaces. We used four intact macropore surfaces of soil clods from each Bt horizon. The surface elevation of 10 surface points per site was measured before and after the manual removal of the outermost surface at an area of 1.350 × 1.012 mm (1.366 mm^2) each. Rip fences were installed at the microscope table to ensure the recovery of the area's XY position. The detection range of the laser beam in the z axis (i.e., the minimum and maximum sample elevation in relation to the microscope's objective) was constant before and after the surface removal. Potentially, a removal of surface layers up to ~2-mm thickness can be considered by this approach (Beck-Broichsitter, Gerriets, Puppe, et al., 2020). Note that the values obtained with this method reflect the thickness of the manually separated material for which the OC contents and CEC have been analyzed (Leue et al., 2018, Leue, Beck-Broichsitter, et al., 2019), rather than that of pure coating material (details in Section 4.2).

2.7 | Quantification of volume-related organic carbon and cation exchange capacity

The bulk soil mass of the entire cylindrical core (M_{core}) with a diameter (d) of 182 mm was calculated as

$$M_{core} = V_{core}\rho = nh\frac{\pi}{4}d^2\rho \quad (3)$$

TABLE 2 Data of organic C (OC) contents (Leue et al., 2018) and effective cation exchange capacity (CEC; Leue, Beck-Broichsitter, et al., 2019) of the bulk soil and separated macropore surface material

Material	OC		CEC	
	Loess-Bt	Till-Bt	Loess-Bt	Till-Bt
	mass %		cmol 100 g^{-1} soil	
Bulk soil (bulk)	0.48	0.34	23	14
Soil matrix (Mx)	0.39	0.24	19	11
Cracks (Cr)	0.92	0.53	23	15
Pinhole fillings (PIN)	1.44	0.77	38	29
Biopore walls (Biop)	0.92	0.53	19	10

where V_{core} is the core volume (cm^3), here determined from the number of image slices (n) of a vertical resolution (h) of $h = 0.231$ mm, and ρ is a site-specific mean dry bulk density (g cm^{-3}) of the soil determined gravimetrically from 100-cm^3 cores assuming that it is identical with the bulk density of the macropore surface layer as a first approximation (details in Section 4.2).

The relative macropore volume (MPV) was calculated from the classified object volumes (in vx) as

$$\mathrm{MPV}\ (\%) = \left(\frac{\sum V_{\mathrm{Biop}} + \sum V_{\mathrm{Cr}}}{V_{\mathrm{Core}}} \right) 100 \tag{4}$$

where subscript "Biop" denotes biopores and subscript "Cr" means cracks and interaggregate spaces.

The pore surface area (S_{Pores} in cm^2) was obtained from the classified object surfaces as

$$S_{\mathrm{Pores}} = \sum S_{\mathrm{Biop}} + \sum S_{\mathrm{Cr}} \tag{5}$$

The mass of the separated surface layer material (M_{surf} in g) was calculated as

$$M_{\mathrm{surf}} = S_{\mathrm{Pores}} \times \mathrm{Lay} \times \rho \tag{6}$$

where Lay is mean thickness (in cm) of the separated macropore surface layer determined by CLSM technique, and ρ is the site-specific mean dry bulk density (g cm^{-3}).

For the entire soil cores, the mass content of organic C (OC_{Core}) and the effective cation exchange capacity (CEC_{Core}) was obtained from the bulk soil data (subscript "bulk") of OC (Leue et al., 2018; Table 2) and CEC (Leue, Beck-Broichsitter, et al., 2019; Table 2; cmol 100 g^{-1} soil) as

$$\mathrm{OC}_{\mathrm{Core}} = M_{\mathrm{Core}} \mathrm{OC}_{\mathrm{bulk}} \tag{7a}$$

$$\mathrm{CEC}_{\mathrm{Core}} = M_{\mathrm{Core}} \mathrm{CEC}_{\mathrm{bulk}} \tag{7b}$$

For the soil matrix (Mx), the total contents of $OC_{Mx(Core)}$ (in g) and $CEC_{Mx(Core)}$ (in cmol) per soil core were calculated as

$$\mathrm{OC}_{\mathrm{Mx(Core)}} = (M_{\mathrm{Core}} - M_{\mathrm{surf}})\, \mathrm{OC}_{\mathrm{Mx}} \tag{8a}$$

$$\mathrm{CEC}_{\mathrm{Mx(Core)}} = (M_{\mathrm{Core}} - M_{\mathrm{surf}})\, \mathrm{CEC}_{\mathrm{Mx}} \tag{8b}$$

For OC_{Mx} and CEC_{Mx}, the data published in Leue et al. (2018) and Leue, Beck-Broichsitter, et al., (2019) were used. Note that the soil matrix (Mx) was denoted as "CS" in these studies.

The contents of OC (g) and CEC (cmol) of the biopore surface material of the cores were determined using the specific masses of biopore surfaces [$M_{surf(Biop)}$] of each core. The OC_{Biop} and CEC_{Biop} values from our own previous works (Leue et al., 2018; Leue, Beck-Broichsitter, et al., 2019) were used:

$$\mathrm{OC}_{\mathrm{Biop(Core)}} = M_{\mathrm{surf(Biop)}} \mathrm{OC}_{\mathrm{Biop}} \tag{9a}$$

$$\mathrm{CEC}_{\mathrm{Biop(Core)}} = M_{\mathrm{surf(Biop)}} \mathrm{CEC}_{\mathrm{Biop}} \tag{9b}$$

Analogously, OC (g) and CEC (cmol) contents of the crack surface material including the coatings, subscript "Cr," were calculated per soil total core as

$$\mathrm{OC}_{\mathrm{Cr(Core)}} = M_{\mathrm{surf(Cr)}} \mathrm{OC}_{\mathrm{Cr}} \tag{10a}$$

$$\mathrm{CEC}_{\mathrm{Cr(Core)}} = M_{\mathrm{surf(Cr)}} \mathrm{CEC}_{\mathrm{Cr}} \tag{10b}$$

The calculation of absolute OC and CEC values of single, disconnected pores ("pinholes," PIN) was not possible in the same way, since the pinholes could not be identified in the XRCT 3D images due to the limited spatial resolution. For an indirect determination of the proportion of PIN in

the OC and CEC of the soil cores, a relation (f, dimensionless) was used (Leue, Beck-Broichsitter, et al., 2019):

$$f_{OC} = \frac{(OC_{bulk} - OC_{Mx})}{(OC_{PIN} - OC_{Mx})} \quad (11a)$$

$$f_{CEC} = \frac{(CEC_{bulk} - CEC_{Mx})}{(CEC_{PIN} - CEC_{Mx})} \quad (11b)$$

which considers the differences in OC contents and CEC between bulk soil (bulk) and soil matrix (Mx) from those between pinholes and matrix. For the loess-Bt, $f_{OC} = 0.048$ and $f_{CEC} = 0.23$, and for the till-Bt, $f_{OC} = 0.132$ and $f_{CEC} = 0.20$. The total OC contents (g) and CEC (cmol) of the pinholes in the soil core were calculated as

$$OC_{PIN} = OC_{Core} f_{OC} \quad (12a)$$

$$CEC_{PIN} = CEC_{Core} f_{CEC} \quad (12b)$$

Finally, all calculated OC and CEC data were related to a soil volume of 1,000 cm^3 in order to allow for a straightforward extrapolation of the data to soil volumes in prospective works.

The difference between the "mean" bulk soil OC and CEC values (bulk) obtained by extrapolating the analytical data of mixed samples to the total soil core, and the sum of the individual components (comps) obtained by combining the surface areas with the contents of the macropore types (Biop, Cr), pinhole fillings (PIN), and the soil matrix (Mx), was calculated in mass % (OC) and cmol 100 g^{-1} soil (CEC) as

$$\begin{aligned}\Delta OC &= OC_{bulk} - OC_{comps} \\ &= OC_{bulk} - \left(OC_{Biop} + OC_{Cr} + OC_{PIN} + OC_{Mx}\right)\end{aligned} \quad (13a)$$

$$\begin{aligned}\Delta CEC &= CEC_{bulk} - CEC_{comps} \\ &= CEC_{bulk} - \left(CEC_{Biop} + CEC_{Cr} + CEC_{PIN} + CEC_{Mx}\right)\end{aligned} \quad (13b)$$

and expressed as percentage related to the bulk soil values.

3 | RESULTS

3.1 | Macropore properties

Under the given XRCT measurement resolution of 0.231-mm vx-edge length and the described image analysis workflow, the total number of recorded objects (i.e., pores or pore segments) was higher for the loess-Bt cores (mean sum of biopores and cracks: 720,162) as compared with the till-Bt cores (mean: 633,945) (Table 3). The loess cores revealed higher proportions in biopore numbers, in particular in the medium and large volume size classes, compared with the till cores (Figure 4). The recorded objects provided mean macropore volumes (MPV) of 5.60% (loess) and 4.62% (till) with relatively high proportions of biopores (loess: 88–99%, till: 67–87%) in each volume size class. Large pores with volumes >0.1 cm^3 represented the largest fraction of the MPVs.

The mean summed surface area of all macropores (biopores and cracks) was ~15,549 cm^2 (loess) and 13,217 cm^2 (till) per soil core (Table 3). Among these surfaces, approximately one-half (loess) and one-third (till) was provided by the largest pores, again with large proportions of biopores (loess: 99%, till: 74%). The mean values of the surface/volume ratio (S/V ratio) were smaller for biopores than for cracks, independent of site or volume size class. The relative differences in S/V ratios between biopores and cracks increased for larger volume size classes. The mean tortuosity (τ), as well as the mean equivalent hydraulic radius (EHR), each increased with the volume size class by one and two magnitudes, respectively, and were at similar levels for samples from loess and till.

3.2 | Organic carbon and cation exchange capacity quantities of macropore surfaces

The thickness of the separated macropore surfaces was 0.56 (±0.26) mm for the loess-Bt samples and 0.66 (±0.36) mm for the till-Bt samples. Mean bulk densities were 1.53 (±0.03) g cm^{-3} for the loess-Bt and 1.77 (±0.06) g cm^{-3} for the till-Bt.

For the bulk soil, the mean OC_{bulk} contents in the scanned soil cores were 7.34 g (loess-Bt) and 6.02 g (till-Bt) per 1,000 cm^3 (Figure 5a). Bulk soil mean CEC values were 35.19 cmol (loess-Bt) and 24.78 cmol (till-Bt) per 1,000 cm^3 soil (Figure 5b). The OC contents and CEC values of the individual components for all macropore surface types and the soil matrix added up to almost the values determined from bulk soil samples (Figure 5). The difference ΔOC between OC_{bulk} and OC_{comps} (Equation 13a) was +1.1% for the loess-Bt and −4.2% for the till-Bt. For the CEC, this difference ΔCEC between CEC_{bulk} and CEC_{comps} (Equation 13b) was +5.8% for the loess-Bt cores and +0.1% for the till-Bt cores. Macropore surfaces accounted for one-third of the OC content and CEC values. From all macropore surface types, the large biopores ($V > 0.1$ cm^3) and pinhole fillings contributed most to the total OC content and CEC (Table 4).

TABLE 3 Basic parameters of the three-dimensional subdatasets of biopores (Biop) and cracks and inter-aggregate spaces (Cr) considering all pores (all), medium-sized pores (medium) with volumes >0.01 to ≤0.1 cm^3 (> 811 to ≤8,113 voxels [vx]), and large pores with volumes >0.1 cm^3 (8,113 vx). Mean values, SDs (in parentheses), and CVs from three soil cores per site are shown

			No. of pores		MPV		Pore surface		*S*/*V* ratio		Tortuosity		EHR	
Site	**Size class**	**Pore type**	**Mean (SD)**	**CV**	**Mean (SD)**	**CV**	**Mean (SD)**	**CV**	**Mean (SD)**	**CV**	**Mean (SD)**	**CV**	**Mean (SD)**	**CV**
			no.		%		cm^2	%		%		%		%
Loess-Bt	All	Biop	450,552 (205,193)	46	5.39 (0.74)	14	14,243 (3,094)	22	2.64 (0.1)	4	4.73 (0.06)	1	1.98 (0.35)	18
		Cr	269,610 (196,479)	73	0.21 (0.18)	86	1,306 (1,124)	86	2.89 (0.04)	1	4.66 (0.02)	0	1.2 (0.07)	6
	Medium	Biop	570 (113)	20	0.2 (0.05)	25	594 (135)	23	1.12 (0.05)	4	10.76 (0.76)	7	33.84 (2.29)	7
		Cr	66 (46)	70	0.03 (0.02)	67	120 (78)	65	1.67 (0.03)	2	26.45 (4.75)	18	31.35 (4.45)	14
	Large	Biop	31 (19)	61	4.32 (0.65)	15	8,905 (2,284)	26	0.8 (0.12)	15	228.89 (206.34)	90	1,106.5 (755.24)	68
		Cr	7 (6)	86	0.02 (0.02)	100	86 (68)	79	1.33 (0.13)	10	57.47 (16.84)	29	118.83 (43.88)	37
	Large/all (%)	Biop	0.004		77.14		57.27							
		Cr	0.001		0.36		0.55							
Till-Bt	All	Biop	118,909 (76,599)	64	3.14 (0.85)	27	6,573 (2,895)	44	2.31 (0.2)	9	4.94 (0.11)	2	3.82 (1.56)	41
		Cr	515,035 (122,790)	24	1.48 (0.6)	41	6,644 (2,344)	35	2.78 (0.03)	1	4.76 (0.02)	0	1.51 (0.1)	7
	Medium	Biop	530 (81)	15	0.22 (0.05)	23	536 (87)	16	1.02 (0.13)	13	8.87 (1.46)	16	39.03 (6.01)	15
		Cr	252 (80)	32	0.11 (0.04)	36	445 (142)	32	1.63 (0.08)	5	27.28 (3.91)	14	35.5 (1.88)	5
	Large	Biop	75 (54)	72	2.37 (0.65)	27	3,578 (1,708)	48	0.6 (0.06)	10	37.35 (25.47)	68	393.41 (130.92)	33
		Cr	36 (1)	3	0.36 (0.07)	19	1,228 (253)	21	1.35 (0.03)	2	94.98 (23.11)	24	196.64 (32.47)	17
	Large/all (%)	Biop	0.012		51.30		27.07							
		Cr	0.006		7.79		9.21							

Note. MPV, macropore volume; *S*/*V*, surface/volume ratio; HER, equivalent hydraulic radius; Large/all, proportion of large biopores or cracks in the total pores (sum of biopores + cracks).

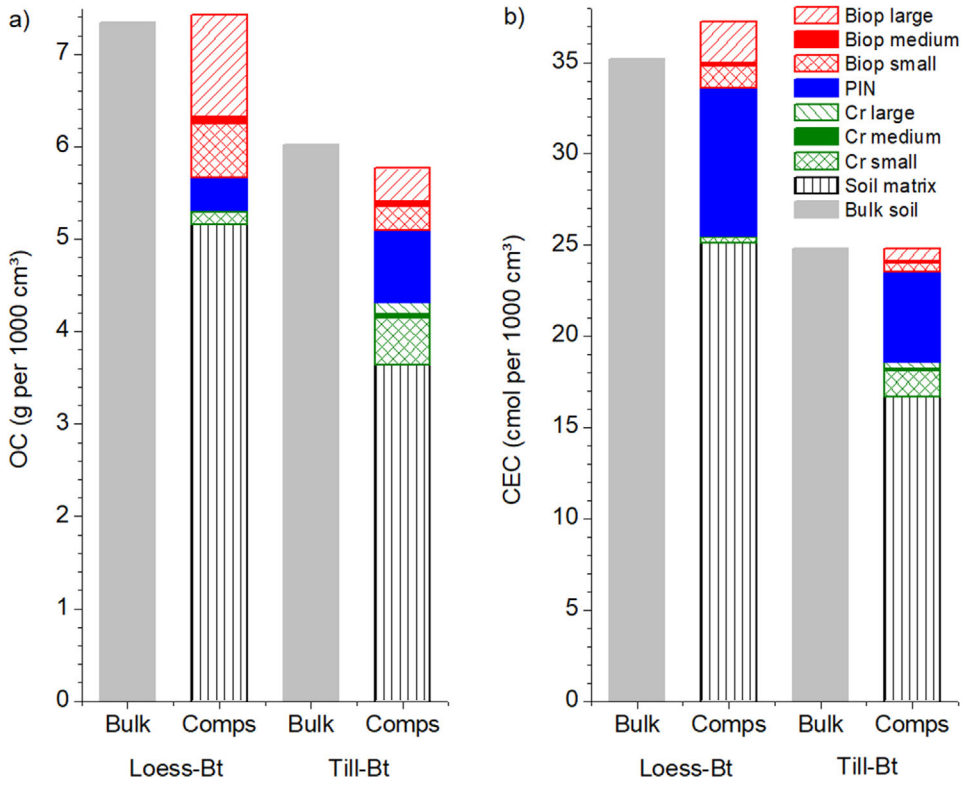

FIGURE 5 (a) Total organic C (OC) content and (b) total cation exchange capacity (CEC) calculated from bulk soil samples (bulk) and the soil components (comps). Comps: soil matrix without macropore surfaces (Mx), separated surface material of the biopores (Biop) and coated cracks (Cr), separated pinhole fillings (PIN), calculated from data of each three soil cores per Bt horizon. Small pore volume = ≤0.01 cm^3, medium pore volume = >0.01 to ≤0.1 cm^3, large pore volume = >0.1 cm^3; contributions of medium and large Cr were partly smaller than symbol sizes

TABLE 4 Relative contributions of the soil components to the organic C (OC) contents and cation exchange capacity (CEC) values of the soil cores and absolute contents of the components per soil volume of 1,000 cm^3. Large biopores and cracks are defined by pore volumes >0.1 cm^3

Soil component	OC relative	OC absolute	CEC relative	CEC absolute
	% of OC sum	g 1,000 cm^{-3}	% of CEC	cmol 1,000 cm^{-3}
Loess-Bt				
Biopores	23.7	1.76	9.7	3.63
Large biopores	14.8	1.10	6.1	2.28
Coated cracks	2.2	0.16	1.1	0.40
Large cracks	0.1	0.01	0.1	0.04
Pinhole fillings	4.7	0.35	21.7	8.09
Soil matrix	69.4	5.15	67.4	25.11
Till-Bt				
Biopores	11.6	0.67	5.1	1.26
Large biopores	6.3	0.36	2.1	0.52
Coated cracks	11.7	0.68	7.7	1.92
Large cracks	2.2	0.13	1.4	0.35
Pinhole fillings	13.6	0.78	20.0	4.96
Soil matrix	63.1	3.64	67.2	16.67

4 | DISCUSSION

4.1 | Relative importance of macropores

The morphological data (Table 3) show that the relatively small numbers, n, of large biopores and cracks (volumes >0.1 cm^3; loess-Bt: n = 38, till-Bt: n = 111) per core provide high proportions in the macropore volume (MPV; loess-Bt: 78%, till-Bt: 59%) in the pore surface (loess-Bt: 58%, till-Bt: 36%). Note that these proportions will be smaller when considering the entire macropore system, including pores smaller than 231 μm, a threshold that was determined here by the XRCT scanning resolution. However, in combination with the EHR values, which were strongly increased as compared with those of smaller macropores ($V \leq 0.01$ cm^3), these data reveal the importance of a few larger macropores, and in particular biopores, for preferential flow and transport processes (Kodešová, Nemecek, Kodeš, & Zigova, 2012; Nobles, Wilding, & Lin, 2010).

The high SDs and CVs of the morphological data (Table 3), in particular of the pore numbers, the MPV, and the pore surfaces, illustrate the differences in the pore systems between the three soil cores. The used soil cores of nearly 25 cm in height and 20 cm in diameter were large compared with those of other XRCT analyses focusing on a differentiation between macropore types (Zhang et al., 2015, 2018). Although the larger cores here were closer to the representative elementary volume, the core size or the number of replicate cores necessary to consider the heterogeneity of the Luvisol Bt horizons were perhaps not sufficient. On the other hand, the core size is limited by the aimed XRCT measurement resolution.

The statistical spread was small for the parameters S/V ratio and tortuosity (Table 3), which can both be used for a differentiation between cylindrical biopores and noncylindrical (i.e., more flat or rounded) cracks and interaggregate spaces (Leue, Ulteau-Puschmann, et al., 2019; Luo et al., 2010). This indicates the suitability of the herein-applied multiscale vessel enhancement filtering for the separation between biopores and nonbiopores in 3D images obtained by XRCT.

In relation to the pore volume (MPV loess: 5.60%, till: 4.62%), macropore surfaces revealed disproportionally higher contents of OC (loess: 31%, till: 37%) and CEC (loess-Bt: 33%, till-Bt: 33%) (Figure 5, Table 4). Biopores dominate the OC storage among the macropore types, which was also reported elsewhere (Beck-Broichsitter, Gerriets, Gerke, et al., 2020). Among the sites, the contributions of crack surfaces and pinhole fillings to the OC contents are larger for the till-Bt than for the loess-Bt. The importance of the macropore wall contribution to the CEC of the Bt horizons is underlined by the fact that macropores often act as preferential root pathways (Kautz, 2015; Ruiz et al., 2015). Both the pathway functions for flow and roots contribute to their role as biogeochemical hotspots of increased turnover (Bundt et al., 2001; Kuzyakov & Blagodatskaya, 2015).

Together with the increased OC contents and CEC along macropores, the OM composition could be important when considering physicochemical properties such as wettability (Leue, Gerke, & Godow, 2015) and sorption (Leue, Beck-Broichsitter, et al., 2019) during water and solute movement along preferential flow paths (van Schaik, Palm, Klaus, Zehe, & Schröder, 2014). Especially for reactive solutes, the local conditions at the macropore surfaces may control sorption and mass exchange between the macropores and the soil matrix (Haas et al., 2020). The here evaluated volume-related properties of macropore type-specific surfaces (Table 4) can be used for a determination of parameters describing domain-specific fractions of pore systems and sorption properties including mass exchange in macroscopic two-domain flow and transport models (Gerke & van Genuchten, 1993; Gerke et al., 2013). The macropore surface areas are representing the maximal size of the macropore–matrix exchange interface and the surface types are related to the structural geometry of this interface (Gerke, 2006). Additional model parameters such as the permeability and diffusivity at the mass exchange interface still need to be determined separately by infiltration and percolation experiments (Fér et al., 2018; Glæsner, Diamantopoulos, Magid, Kjaergaard, & Gerke, 2018). In addition, temporal and spatial effects such as swelling and shrinking and root growth (Schlüter, Albrecht, Schwärzel, & Kreiselmeier, 2020) must be taken into account.

4.2 | Thickness and bulk density of coatings at macropore surfaces

In the presented approach, the thickness of the separated macropore surface layer is greater than the thickness of the coating layers identifiable by visible inspection. Due to the manual sampling procedure, the separated layer often contains some larger particles from the soil matrix next to the coating, which leads to a "dilution effect" (Leue et al., 2018). Only larger pinhole fillings could be separated more easily. The thickness of the separated macropore surface layer depends on the texture (sand grains tend to more disturbances than smaller particles), soil moisture (wetter samples allow for finer separation), and the person in charge.

With a XRCT spatial resolution of 231-μm vx-edge length, it was not possible to directly identify coating layers along crack surfaces from the 3D images. Leue et al. (2018) estimated a coating thickness of 58 μm for the loess-Bt and

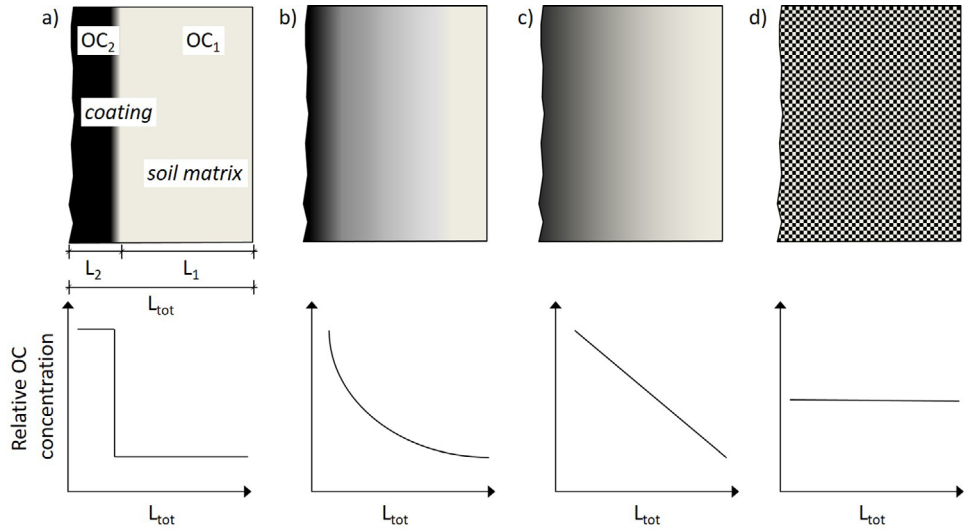

FIGURE 6 Simplified potential depth distributions ("concentration" gradients) of clay-organic-rich coating material (including corresponding organic C [OC] concentration and cation exchange capacity [CEC]) at or within macropore surfaces in a manually separated layer (L_{tot}): (a) clear differentiation between coating (L_2) and underlying soil matrix (L_1), (b) exponential and (c) linear decrease of coating material by depth, (d) homogeneous content of coating material in the separated layer ($L_{tot} = L_2$). OC_1, organic C content of soil matrix; OC_2, organic C content of surface coatings

129 μm for the till-Bt; coating thicknesses between approximately 100 and 500 μm were found by Kodešová et al. (2012) and Beck-Broichsitter, Gerriets, Puppe, et al. (2020). Note that the presence of coating material is not necessarily restricted to the outermost surface of macropores. Coatings may also vary in the thickness as indicated by the high values of the SD of ±38 μm (loess) and ±94 μm (till) for the mean thickness values of 58 μm (loess-Bt) and 129 μm (till-Bt) previously determined by Leue et al. (2018). The data (not shown) from test XRCT measurements of relatively small aggregate samples at spatial resolution of 1–2 μm suggested that the coating thickness as identifiable by XRCT 3D images can be much smaller (i.e., 8–10 μm) than those cited above. In addition, the depth distribution of coating material at or within the macropore surface could have different characteristics that complicate the identification of the coating material in XRCT 3D images. It also complicates the differentiation between OC and CEC values from separated surface layer and from "real" macropore coatings under in situ conditions. Note that OC concentration (Leue et al., 2018) and CEC (Leue, Beck-Broichsitter, et al., 2019) are strongly determined by the content of clay-organic coating or pore filling material. Conceptually, different gradients of coatings at or within the outermost macropore surface layer are possible (Figure 6). The simplest model is an accumulation as a homogenous outermost layer at the macropore surfaces (Figure 6a), resulting in clear differences in OC and CEC values between the coating material enriched in clay minerals and soil OM, and the underlying soil matrix. Alternatively, the "concentration" of accumulated coating material (including corresponding OC concentration and CEC) within macropore surfaces could be an exponential (Figure 6b) or linear decay (Figure 6c). Even a homogenous incorporation (Figure 6d) of coating material in the soil matrix could be possible, assuming intensive mixing and transport due to biological activity and solute movement.

The determination of the bulk density of the separated surface layer using CLSM failed here because the separated surface material from the sampled surface area could not exactly be fitted to the area covered by the CLSM measurement (i.e., the laser beam). In addition, a material loss during the separation could not be avoided. For lack of data, we used the same site-specific bulk density value for both the soil matrix and the separated surface material because it was unclear whether the density of the surface coatings was increased or decreased compared with that of the bulk soil. The density of macropore surfaces can potentially be affected by several factors:

1. Due to the compression of earthworms and roots, the outermost surface layer of biopores can be compacted (i.e., revealing higher bulk density values than the underlying soil matrix; Haas & Horn, 2018; Rogasik, Schrader, Onasch, Kiesel, & Gerke, 2014; Ruiz et al., 2015).
2. Biopore surfaces can be smeared (Jégou, Schrader, Diesel, & Cluzeau, 2001), and the OM accumulation in smaller pores can alter the surface density by clogging smaller pores along macropores

(Pagenkemper et al., 2015), also resulting in a reduced surface roughness of coated cracks (Leue & Gerke, 2016).

3. Since OM has a lower density than mineral matter, the bulk density of macropore surfaces is decreasing in the case of OM accumulation.
4. An increased microbial activity along macropores (Bundt et al., 2001; Kuzyakov & Blagodatskaya, 2015) may result in a higher porosity (i.e., a lower bulk density of macropore surfaces) as compared with the soil matrix.
5. Eventually, increased proportions of clay minerals could decrease the bulk density of coatings compared with that of the quartz-dominated soil matrix (Beck-Broichsitter, Gerriets, Puppe, et al., 2020).

Higher bulk densities (as well as higher coating thicknesses and higher OC and CEC values) of earthworm burrow walls and crack surfaces would increase the relative contribution of these macropore surfaces to contents of OC and CEC within structured soils. For clarifying these points, high-resolution XRCT scans down to spatial resolutions of few micrometers would be necessary.

4.3 | Two-dimensional spatial distribution of coatings along macropore surfaces

An important issue determining the OC and CEC values of macropore surfaces is the spatial extent to which cracks and interaggregate spaces are covered by clay-organic coatings under in situ conditions. Maps of the 2D distribution of OC (Leue et al., 2018) and CEC (Leue, Beck-Broichsitter, et al., 2019) revealed that the spatial distribution of these parameters at intact macropore surfaces is heterogeneous. This local millimeter to centimeter scaled distribution could also affect the macropore–matrix mass exchange for solutes during preferential flow through a highly sensitive diffusive exchange parameter (Gerke et al., 2013). Keck et al. (2017) also showed a heterogeneous distribution of cation adsorption sites, even though at a smaller spatial scale. However, own field observations revealed that nearly all crack surfaces of the two investigated Bt horizons were covered by clay-organic coating material (as visible to the naked eye) in different intensities. For considering heterogeneities in the coating distribution, area-weighted mean OC values for biopore and crack surfaces of 0.92% (loess-Bt) and 0.53% (till-Bt) (Table 2) have been used in this study, based on histograms of the 2D spatial distribution of OC at intact macropore surfaces presented by Leue et al. (2018).

4.4 | Limitations and uncertainties of the approach

Summarizing the methodological issues discussed herein, the presented approach is subjected to the question of representativeness. Besides common uncertainties concerning the measurement data of chemical input parameters (here, OC and CEC), the morphological data of the soil macropores and the occurrence of the macropore surfaces affect the quantification results.

Concerning the morphological data, a tradeoff exists between the sampling of a representative soil volume and the spatial resolution of the XRCT measurement to be achieved. With respect to the macropore surfaces, a divergence between the thickness of the sampled surface layer (several hundred microns) and the actual coating thickness cannot be avoided. In this context, the differentiation between coating layer and the more or less "inactive" underlying soil matrix is not quite clear. Also, the thickness of macropore surface to be considered depends on the scientific question. For example, the wettability of macropore surfaces during preferential flow events can be related to a different surface layer thickness than the OM turnover. In this context, the bulk density of macropore surfaces may affect the quantification results as well. Lastly, uncertainties still exist concerning the extent to which macropore surfaces are covered by coatings.

5 | CONCLUSIONS

Our aim was to quantitatively estimate the OC content and CEC of type-specific coatings at macropore surfaces for the entire volume of intact soil cores. For this purpose, 3D image data from XRCT measurements from two Luvisol Bt horizons (three cores each) were evaluated to separate between biopores and cracks and were combined with coating thickness, OC, and CEC data.

About one-third of the OC contents and CECs of the bulk Bt horizons were calculated for all macropore surfaces, indicating a 5× (loess-Bt) and 6.5× (till-Bt) higher concentration of OC and CEC along macropore surfaces as compared with their volume fractions of 5.6% (loess-Bt) and 4.6% (till-Bt). These results indicate the relative importance of macropore surface properties for biogeochemical and transport processes and confirm conclusions of previous studies. Macropore type- and site-specific OC contents and CEC values along macropore surfaces may help explain differences in flow, transport, and sorption processes between these Bt horizons, as well as in OC storage and biogeochemical turnover processes. Volume-based coating properties may help improve

macroscopic-scale two-domain flow and transport models by providing independently determined information on domain-specific sorption and macropore–matrix mass exchange parameters.

The mass balance of OC contents and CEC values as calculated from bulk soil data and from the sum of the contributions of the soil matrix and the different macropore surface types including the pinhole fillings suggest that the present approach gives reasonable results. Still, a number of methodological issues remain, such as an improved micrometer-scale approach for in situ determination of surface layer thickness and coating bulk density. The relatively pragmatic approach presented may be useful for characterizing a process-oriented effective spatial distribution of biogeochemical hotspots. Further improvements of XRCT measurements and 3D XRCT data analysis may eventually lead to more detailed information on spatially distributed, local, sorption-relevant properties at intact macropore surfaces.

CONFLICT OF INTEREST

The authors declare no conflict of interest.

ACKNOWLEDGMENTS

This study was financially supported by the Deutsche Forschungsgemeinschaft (DFG), Bonn, Germany, under Grants LE 3177/1-2 "Quantification of small-scale physicochemical and microbiological properties of intact macropore surfaces in structured soils," GE 990/10 "SOMATRA," and GE 990/14 "FLEXPO." We thank Radka Kodešová and Miroslav Fér, Czech University of Life Sciences Prague, and Lidia Völker, Jennika Hammar, Ingrid Onasch, Helmut Rogasik, and Norbert Wypler, ZALF Müncheberg, for support with the soil sampling, as well as Jens Nellesen, RIF Dortmund, for the XRCT measurements.

ORCID

Martin Leue https://orcid.org/0000-0002-8392-4545
Horst H. Gerke https://orcid.org/0000-0002-6232-7688

REFERENCES

Beck-Broichsitter, S., Gerriets, M. R., Gerke, H. H., Sobotkova, M., Dusek, J., Dohrmann, R., & Horn, R. (2020). Brilliant Blue sorption characteristics of clay-organic aggregate coatings from Bt horizons. *Soil and Tillage Research*, *201*. https://doi.org/10.1016/j.still.2020.104635

Beck-Broichsitter, S., Gerriets, M. R., Puppe, D., Leue, M., Dusek, J., Sobotková, M., & Gerke, H. H. (2020). Laser-based 3D microscopic gauging of soil macropore coating thickness and volume. *Soil and Tillage Research*, *204*. https://doi.org/10.1016/j.still.2020.104715

Barton, C. D., & Karathanasis, A. D. (1997). Measuring cation exchange capacity and total exchangeable bases in batch and flow experiments. *Soil Technology*, *11*, 153–162. https://doi.org/10.1016/S0933-3630(97)00002-0

Blakemore, L. C., Searle, P. L., & Daly, B. K. (1987). *Methods of chemical analysis of soils*. New Zealand Soil Bureau. http://doi.org/10.7931/DL1-SBSR-10A

Bundt, M., Widmer, F., Pesaro, M., Zeyer, J., & Blaser, P. (2001). Preferential flow paths: Biological 'hot spots' in soils. *Soil Biology and Biochemistry*, *33*, 729–738. https://doi.org/10.1016/S0038-0717(00)00218-2

Capowiez, Y., Sammartino, S., & Michel, E. (2011). Using X-ray tomography to quantify earthworm bioturbation non-destructively in repacked soil cores. *Geoderma*, *162*, 124–131. https://doi.org/10.1016/j.geoderma.2011.01.011

Don, A., Steinberg, B., Schöning, I., Pritsch, K., Joschko, M., Gleixner, G., & Schulze, E.-D. (2008). Organic carbon sequestration in earthworm burrows. *Soil Biology and Biochemistry*, *40*, 1803–1812. https://doi.org/10.1016/j.soilbio.2008.03.003

Feldkamp, L. A., Davis, L. C., & Kress, J. W. (1984). Practical cone-beam algorithm. *Journal of the Optical Society of America A*, *1*, 612–619. https://doi.org/10.1364/JOSAA.1.000612

Fér, M., Kodešová, R., Golovko, O., Schmidtová, Z., Klement, A., Nikodem, A., … Grabic, R. (2018). Sorption of atenolol, sulfamethoxazole and carbamazepine onto soil aggregates from the illuvial horizon of the Haplic Luvisol on loess. *Soil and Water Research*, *13*, 177–183. https://doi.org/10.17221/82/2018-SWR

Frangi, A. F., Niessen, W. J., Vincken, K. L., & Viergever, M. A. (1998). Multiscale vessel enhancement filtering. In W. M. Wells, A. Colchester, & S. Delp. (Eds.), *Medical image computing and computer-assisted intervention: MICCAI'98* (pp. 130–137). Berlin, Heidelberg: Springer.

Fraunhofer ITWM. (2012). MAVI: Modular Algorithms for Volume Images. Version 1.4.1. Kaiserslautern, Germany: Fraunhofer Institute for Industrial Mathematics.

Gerke, H. H., & van Genuchten, M. T. (1993). A dual-porosity model for simulating the preferential movement of water and solutes in structured porous media. *Water Resources Research*, *29*, 305–319. https://doi.org/10.1029/92WR02339

Gerke, H. H. (2006). Preferential flow descriptions for structured soils. *Journal of Plant Nutrition and Soil Science*, *169*, 382–400. https://doi.org/10.1002/jpln.200521955

Gerke, H. H. (2012). Macroscopic representation of the interface between flow domains in structured soil. *Vadose Zone Journal*, *11*(3). https://doi.org/10.2136/vzj2011.0125

Gerke, H. H., Dusek, J., & Vogel, T. (2013). Solute mass transfer effects in two-dimensional dual-permeability modeling of bromide leaching from a tile-drained field. *Vadose Zone Journal*, *12*(2). https://doi.org/10.2136/vzj2012.0091

Glæsner, N., Diamantopoulos, E., Magid, J., Kjaergaard, C., & Gerke, H. H. (2018). Modeling solute mass exchange between pore regions in slurry injected soil columns during intermittent irrigation. *Vadose Zone Journal*, *17*(1). https://doi.org/10.2136/vzj2018.01.0006

Haas, C., & Horn, R. (2018). Impact of small-scaled differences in micro-aggregation on physico-chemical parameters of macroscopic biopore walls. *Frontiers in Environmental Science*, *6*. https://doi.org/10.3389/fenvs.2018.00090

Haas, C., Horn, R., Ellerbrock, R. H., & Gerke, H. H. (2020). Fluorescence imaging for mm-scale observation of macropore-matrix mass transfer: Calibration experiments. *Geoderma*, *360*. https://doi.org/10.1016/j.geoderma.2019.114002

IUSS Working Group WRB. (2006). *World reference base for soil resources 2006: A framework for international classification, correlation and communication*. Rome: FAO.

Jarvis, N. (2007). A review of non-equilibrium water flow and solute transport in soil macropores: Principles, controlling factors and consequences for water quality. *European Journal of Soil Science*, *58*, 523–546. https://doi.org/10.1111/j.1365-2389.2007.00915.x

Jégou, D., Schrader, S., Diesel, H., & Cluzeau, D. (2001). Morphological, physical and biochemical characteristics of burrow walls formed by earthworms. *Applied Soil Ecology*, *17*, 165–174. https://doi.org/10.1016/S0929-1393(00)00136-0

Kautz, T. (2015). Research on subsoil biopores and their functions in organically managed soils: A review. *Renewable Agriculture and Food Systems*, *30*, 318–327. https://doi.org/10.1017/S1742170513000549

Keck, H., Strobel, B. W., Gustafsson, J. P., & Koestel, J. (2017). Quantitative imaging of the 3-D distribution of cation adsorption sites in undisturbed soil. *SOIL*, *3*, 177–189. https://doi.org/10.5194/soil-3-177-2017

Kodešová, R., Nemecek, K., Kodeš, V., & Zigova, A. (2012). Using dye tracer for visualization of preferential flow at macro- and microscales. *Vadose Zone Journal*, *11*(1). https://doi.org/10.2136/vzj2011.0088

Kuzyakov, Y., & Blagodatskaya, E. (2015). Microbial hotspots and hot moments in soil: Concept & review. *Soil Biology and Biochemistry*, *83*, 184–199. https://doi.org/10.1016/j.soilbio.2015.01.025

Leue, M., Beck-Broichsitter, S., Felde, V. J. M. N. L., & Gerke, H. H. (2019a). Determining mm-scale maps of cation exchange capacity at macropore surfaces in Bt-horizons. *Vadose Zone Journal*, *18*(1). https://doi.org/10.2136/vzj2018.08.0162

Leue, M., Eckhardt, K.-U., Ellerbrock, R. H., Gerke, H. H., & Leinweber, P. (2016). Analyzing organic matter composition at intact biopore and crack surfaces by combining DRIFT spectroscopy and pyrolysis-field ionization mass spectrometry. *Journal of Plant Nutrition and Soil Science*, *179*, 5–17. https://doi.org/10.1002/jpln.201400620

Leue, M., Eckhardt, K.-U., Gerke, H. H., Ellerbrock, R. H., & Leinweber, P. (2017). Spatial distribution of organic matter compounds at intact macropore surfaces predicted by DRIFT spectroscopy. *Vadose Zone Journal*, *16*(9). https://doi.org/10.2136/vzj2017.05.0111

Leue, M., & Gerke, H. H. (2016). Roughness of biopores and cracks in Bt-horizons assessed by confocal laser scanning microscopy. *Journal of Plant Nutrition and Soil Science*, *179*, 529–536. https://doi.org/10.1002/jpln.201600016

Leue, M., Gerke, H. H., & Godow, S. C. (2015). Droplet infiltration and organic matter composition of intact crack and biopore surfaces from clay-illuvial horizons. *Journal of Plant Nutrition and Soil Science*, *178*, 250–260. https://doi.org/10.1002/jpln.201400209

Leue, M., Uteau-Puschmann, D., Peth, S., Nellesen, J., Kodešová, R., & Gerke, H. H. (2019). Separation of soil macropore types in 3D X-ray CT-images based on pore geometry characteristics. *Vadose Zone Journal*, *18*(1). https://doi.org/10.2136/vzj2018.09.0170

Leue, M., Wohld, A., & Gerke, H. H. (2018). Two-dimensional distribution of soil organic carbon at intact macropore surfaces in Bt-horizons. *Soil and Tillage Research*, *176*, 1–9. https://doi.org/10.1016/j.still.2017.10.002

Lin, H. (2010). Linking principles of soil formation and flow regimes. *Journal of Hydrology*, *393*, 3–19. https://doi.org/10.1016/j.jhydrol.2010.02.013

Luo, L., Lin, H., & Li, S. (2010). Quantification of 3-D soil macropore networks in different soil types and land uses using computed tomography. *Journal of Hydrology*, *393*, 53–64. https://doi.org/10.1016/j.jhydrol.2010.03.031

Nobles, M. M., Wilding, L. P., & Lin, H. S. (2010). Flow pathways of bromide and brilliant blue FCF tracers in caliche soils. *Journal of Hydrology*, *393*, 114–122. https://doi.org/10.1016/j.jhydrol.2010.03.014

Otsu, N. (1979). A threshold selection method from gray-level histograms. *IEEE Transactions on Systems, Man, and Cybernetics*, *9*, 62–66. https://doi.org/10.1109/TSMC.1979.4310076

Pagenkemper, S. K., Athmann, M., Uteau-Puschmann, D., Kautz, T., Peth, S., & Horn, R. (2015). The effect of earthworm activity on soil bioporosity: Investigated with X-ray computed tomography and endoscopy. *Soil and Tillage. Research*, *146*, 79–88. https://doi.org/10.1016/j.still.2014.05.007

Pagenkemper, S. K., Peth, S., Uteau-Puschmann, D., & Horn, R. (2013). Effects of root-induced biopores on pore space architecture investigated with industrial X-ray computed tomography. In S. H. Anderson & J. W. Hopmans (Eds.), *Soil-water-root processes: Advances in tomography and imaging* (Vol. 61). Madison, WI: SSSA. https://doi.org/10.2136/sssaspecpub61.c4

Perret, J., Prasher, S. O., Kantzas, A., & Langford, C. (1999). Three-dimensional quantification of macropore networks in undisturbed soil cores. *Soil Science Society of America Journal*, *63*, 1530–1543. https://doi.org/10.2136/sssaj1999.6361530x

Pierret, A., Capowiez, Y., Belzunces, L., & Moran, C. J. (2002). 3D reconstruction and quantification of macropores using X-ray computed tomography and image analysis. *Geoderma*, *106*, 247–271. https://doi.org/10.1016/S0016-7061(01)00127-6

Rogasik, H., Schrader, S., Onasch, I., Kiesel, J., & Gerke, H. H. (2014). Micro-scale dry bulk density variation around earthworm (*Lumbricus terrestris* L.) burrows based on X-ray computed tomography. *Geoderma*, *213*, 471–477. https://doi.org/10.1016/j.geoderma.2013.08.034

Rogasik, H., Weinkauf, H., & Seyfarth, M. (1997). Methodology and technology of sampling undisturbed soil cores. (In German, with English abstract.) *Archives of Agronomy and Soil Science*, *41*, 199–207. https://doi.org/10.1080/03650349709365991

Ruiz, S., Or, D., & Schymanski, S. J. (2015). Soil penetration by earthworms and plant roots: Mechanical energetics of bioturbation of compacted soils. *PLOS ONE*, *10*(9). https://doi.org/10.1371/journal.pone.0128914

Sammartino, S., Lissy, A.-S., Bogner, C., Van Den Bogaert, R., Capowiez, Y., Ruy, S., & Cornu, S. (2015). Identifying the functional macropore network related to preferential flow in structured soils. *Vadose Zone Journal*, *14*(10). https://doi.org/10.2136/vzj2015.05.0070.

Sato, Y., Nakajima, S., Shiraga, N., Atsumi, H., Yoshida, S., Koller, T., … Kikinis, R. (1998). Three-dimensional multi-scale line filter for segmentation and visualization of curvilinear structures in medical images. *Medical Image Analysis*, *2*, 143–168. https://doi.org/10.1016/S1361-8415(98)80009-1

Schlüter, S., Albrecht, L., Schwärzel, K., & Kreiselmeier, J. (2020). Long-term effects of conventional tillage and no-tillage on saturated and near-saturated hydraulic conductivity: Can their prediction be improved by pore metrics obtained with X-ray CT? *Geoderma*, *361*. https://doi.org/10.1016/j.geoderma.2019.114082

van Schaik, L., Palm, J., Klaus, J., Zehe, E., & Schröder, B. (2014). Linking spatial earthworm distribution to macropore numbers and hydrological effectiveness. *Ecohydrology*, *7*, 401–408. https://doi.org/10.1002/eco.1358

Zhang, Z., Liu, K., Zhou, H., Lin, H., Li, D., & Peng, X. (2018). Three dimensional characteristics of biopores and non-biopores in the subsoil respond differently to land use and fertilization. *Plant and Soil*, *428*, 453–467. https://doi.org/10.1007/s11104-018-3689-3

Zhang, Z. B., Peng, X., Zhou, H., Lin, H., & Sun, H. (2015). Characterizing preferential flow in cracked paddy soils using computed tomography and breakthrough curve. *Soil and Tillage Research*, *146*, 53–65. https://doi.org/10.1016/j.still.2014.05.016

How to cite this article: Leue M, Uteau D, Peth S, Beck-Broichsitter S, Gerke HH. Volume-related quantification of organic carbon content and cation exchange capacity of macropore surfaces in Bt horizons. *Vadose Zone J.* 2020;19:e20069. https://doi.org/10.1002/vzj2.20069